Supporting Information

Short and soft: multi-domain organization, tunable dynamics and jamming in suspensions of grafted colloidal cylinders with small aspect ratio

Daniele Parisi[1,2], Yingbo Ruan[3,4], Guy Ochbaum[5], Kevin S. Silmore[6], Lucas L. Cullari[5], Chen-Yang Liu[3,4], Ronit Bitton[5], Oren Regev[5], James W. Swan[6], Benoit Loppinet[1] and Dimitris Vlassopoulos[1,2]

1 Institute of Electronic Structure & Laser, FORTH, Heraklion 71110, Crete, Greece

2 Department of Materials Science & Technology, University of Crete, Heraklion 71003, Crete, Greece

3 Beijing National Laboratory for Molecular Sciences, CAS Key Laboratory of Engineering Plastics, Institute of Chemistry, The Chinese Academy of Sciences, Beijing 100190, China

4 University of Chinese Academy of Sciences, Beijing 100049, China

5 Department of Chemical Engineering and the Ilze Katz Institute for Nanoscale Science & Technology, Ben-Gurion University of the Negev, Beer-Sheva 84105, Israel

6 Department of Chemical Engineering, Massachusetts Institute of Technology, Cambridge, MA, 02139, USA

Contents

SI1. Analysis of polydispersity

Figure S1 shows the form factor of the cylinders obtained by combining different scattering techniques. The intensity is normalized by that of the solvent (diethyl phthalate in this case) and divided by the concentration. Data points have been fitted with a form factor for core-shell cylinders implemented in the open source SASfit software (https://sourceforge.net/projects/sasfit/) developed by Joachim Kohlbrecher of Paul Scherrer Institute, Villigen, Switzerland (see red solid line in figure S1). Fitting parameters were: radius of the core+shell, grafting density, length, solvency conditions, polydispersity, scattering length densities of core, solvent and shell. The length and the diameter estimated by the fitting routine are respectively 720 nm and 121 nm. The estimated polydispersity is 1.22. The obtained values are in very good agreement with those estimated through TEM images (see main text). Indeed, cryo-TEM measurements confirmed the shape and size of the investigated nanocylinders in solution, meaning that the drying process does not affect much the structure and stability of the nanocylinders.

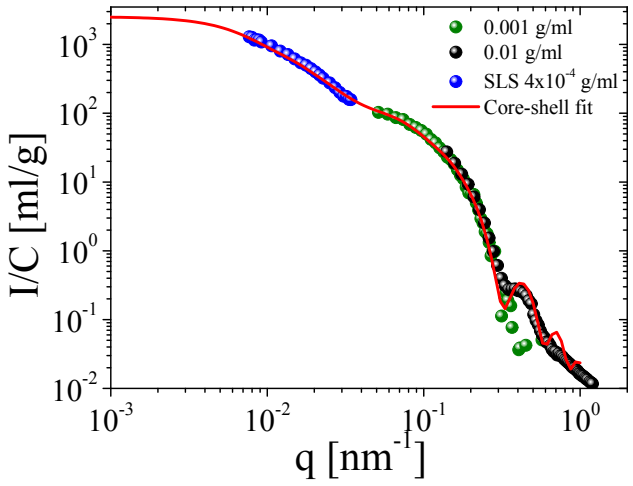

Figure S1. Form factor obtained from static light (blue solid circles) and X-ray (green and black circles) scattering experiments in diethyl phthalate (DEP). Solid red line shows the core-shell model fit for cylindrical particles.

Alternatively, using the analytical expressions for the light scattering time autocorrelation function of Schulz-distributed Rayleigh-Debye particles proposed by Aragon and R. Pecora[1] we arrive at a polydispersity value of 1.21. However, we note that such a model is expected to be valid for Gaussian coils and thin rods.

Interestingly, the polydispersity exceeds 18%, which is the threshold limit predicted by Bates and Frenkel for the destabilization of mesophases.[2]

SI2. Sizes in different solvents

Figure S2 below depicts the hydrodynamic and gyration radii in three different solvents (Toluene, Diethyl Phthalate and Dioctyl Phthalate) of spherical micelles with the same chemistry, same graft molar mass and similar grafting density,[3] at different temperatures. Our goal is to obtain indirect information about solvent quality effects, i.e., relative size in different solvents, which is not affected by the shape for the same molar mass and grafting density of the shell. Here, we refer only on the different particle sizes in different solvents. Clearly at 25 ^{0}C the PS shell is swollen in both toluene and DEP.

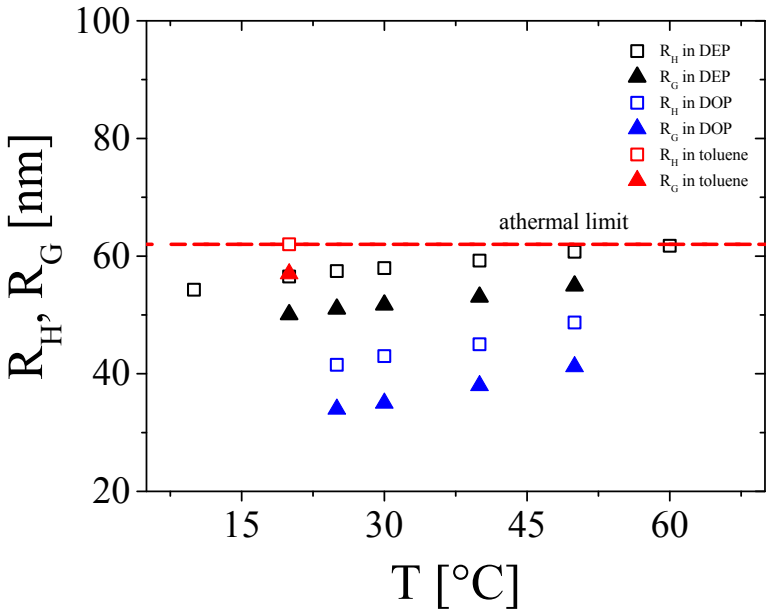

Figure S2. Temperature dependence of the hydrodynamic radius and radius of gyration in different solvents for spherical micelles with the same PS graft molar mass (111 kg/mol) and nearly the same grafting density (0.075 chains/nm^2). The dashed red line marks the athermal limit reached with the suspension in toluene.

SI3. Dynamic light scattering characterization

Data in the dilute regime (4x10^{-4} g/ml) are shown in Figure S3. Correlation functions exhibit only one decay process at different angles, from 30° to 150°. This is also confirmed quantitatively by the values of the stretched exponents found through the Kohlrausch-Williams-Watts (KWW) stretched exponential fit function.[4] The ratio between the decay rate Γ and the squared value of the scattering wave vector was found independent from the scattering wave vector, typical of diffusive motion, with a resulting diffusion coefficient 1x10^{-13} m^2/s.

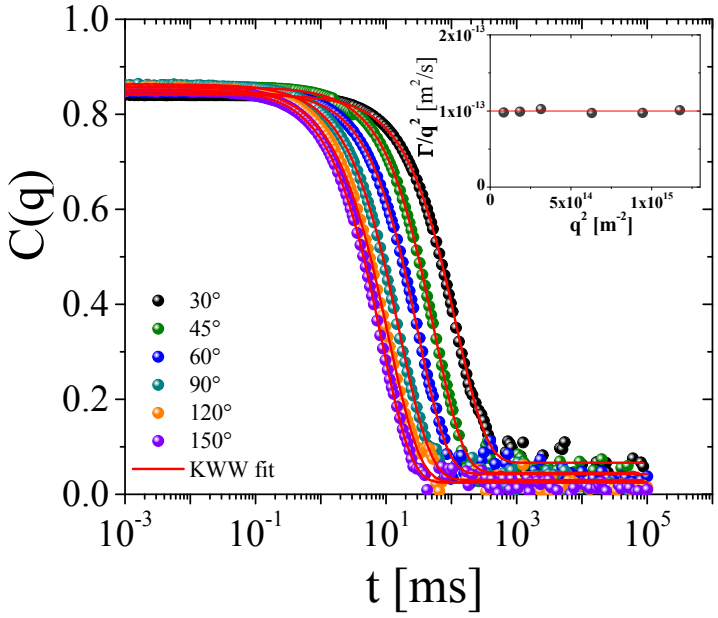

Figure S3. Normalized electric field time auto-correlation functions at six different scattering angles fitted with the Kohlrausch-Williams-Watts (KWW) stretched exponential function (red lines). The concentration is $4x10^{-4}$ g/ml (dilute regime). Stretched exponents have value of 1. The inset shows the dependence of the ratio between the decay rate Γ and the squared value of the scattering wave vector on the scattering wave vector.

The onset of the nonergodicity was monitored by means of dynamic light scattering experiments in toluene (Figure S4). Fitting with the KWW function provides the evolution of the broadness of the correlation functions with concentration. A stretched exponent equal to 0.5 coincides with the onset of nonergodicity as it was also observed in fd-viruses.[5]

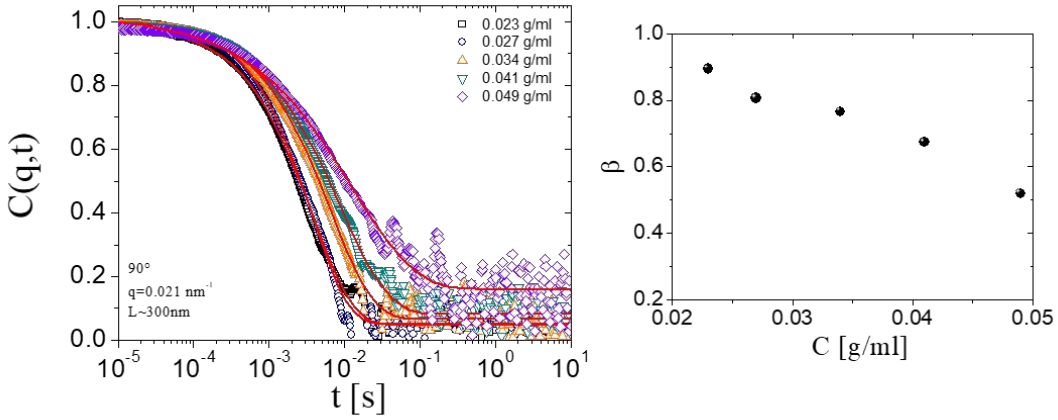

Figure S4. Left panel: Normalized electric field auto-correlation functions of cylindrical nanoparticles in toluene at different concentrations and at a scattering wave vector equal to $0.021nm^{-1}$. Red solid lines represent fitting curves with a stretched exponential function. Right Panel: Concentration dependence of the stretched exponent β.

SI4. Shell thickness

For grafted cylinders where the core radius is much larger than the size of a monomer but smaller than the shell thickness, Binder et al.[6] proposed the following relation to roughly estimate the shell thickness in good solvency conditions:

$$h = ab(\sigma b^2)^{0.259}(\mathrm{M}_n/\mathrm{M}_0)^{0.74} \qquad \text{(S1)}$$

where σ is the grafting density at the core, M_n and M_0 being the molar masses of the grafted chain (111 kg/mol) and Kuhn monomer (0.720 kg/mol[7]), whereas b is the Kuhn monomer size (b=1.8 nm[7]) and a is a proportionality constant of order 1, which for simplicity is assumed equal to 1. Equation S1 yields a value of 56 nm.

SI5. Transmission Electron Microscopy

Figure S5 depicts the Transmission Electron Microscopy (TEM) and cryo-TEM images of the investigated suspensions. Indeed, TEM images where used to estimate the average particle length and its polydispersity (average of more than 10 images). Typical results are shown in Figure S5. A cryo-TEM image at 0.01 g/ml in DEP is reported as well to show that systems are also stable in solution keeping their cylindrical shape and arranging into domains with no prevalent orientational direction.

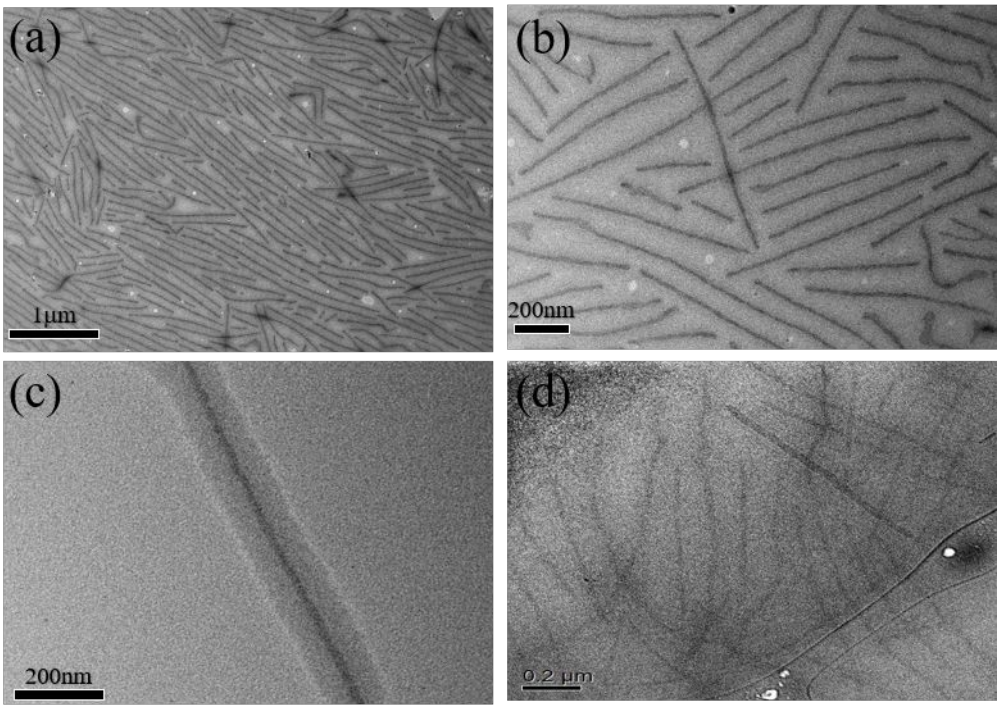

Figure S5. (a-c) TEM images at 3 different magnifications. In panel (c) a single particle with detectable core-shell contrast is observed. d) Cryo-TEM image of cylinders in DEP at 0.01 g/ml.

SI6. Small angle X-ray scattering (SAXS)

Results from SAXS measurements performed on a self-assembled film[3] are shown in Figure S6. They display structural peaks (not too sharp though) compatible with a hexagonal crystalline structure. The dynamic moduli reported in the main text at C=0.76 g/ml exhibit a 1/3 slope against frequency, which is expected for hexagonally packed cylinders.[8] Nevertheless, the possibility of having such a pure crystalline state is rather small because of the non-negligible polydispersity in length of the investigated short cylinders.

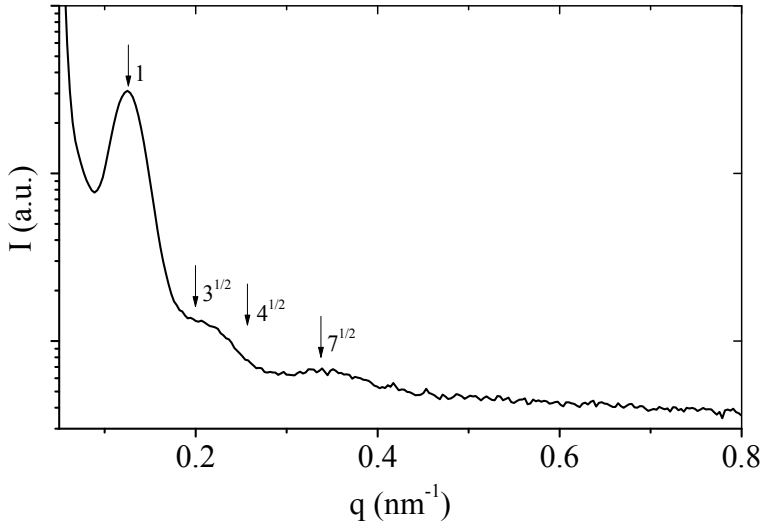

Figure S6. X-ray scattering intensity of the self-assembled film in solvent-free conditions. Black arrows point peak positions of a hexagonal crystalline structure.

SI7. Creep measurements

Figure S7 shows creep compliances at various concentrations. Applied stresses range from 1 Pa for the lowest concentration (0.1 g/ml) to 50 Pa for the highest concentration (0.6 g/ml). Error bars were calculated through 3 different measurements at different stresses per concentration to ensure that the rheological response is within the linear viscoelastic regime. The conversion of the creep compliance into dynamic moduli was obtained by using the regularization method for nonlinear-ill posed problems (NLREG) proposed by Weese et al.[9–12] The NLREG software, based on the original Tikhonov regularization method, evaluates the retardation spectrum from creep compliance and subsequently calculates the relaxation spectrum and the associated viscoelastic functions.

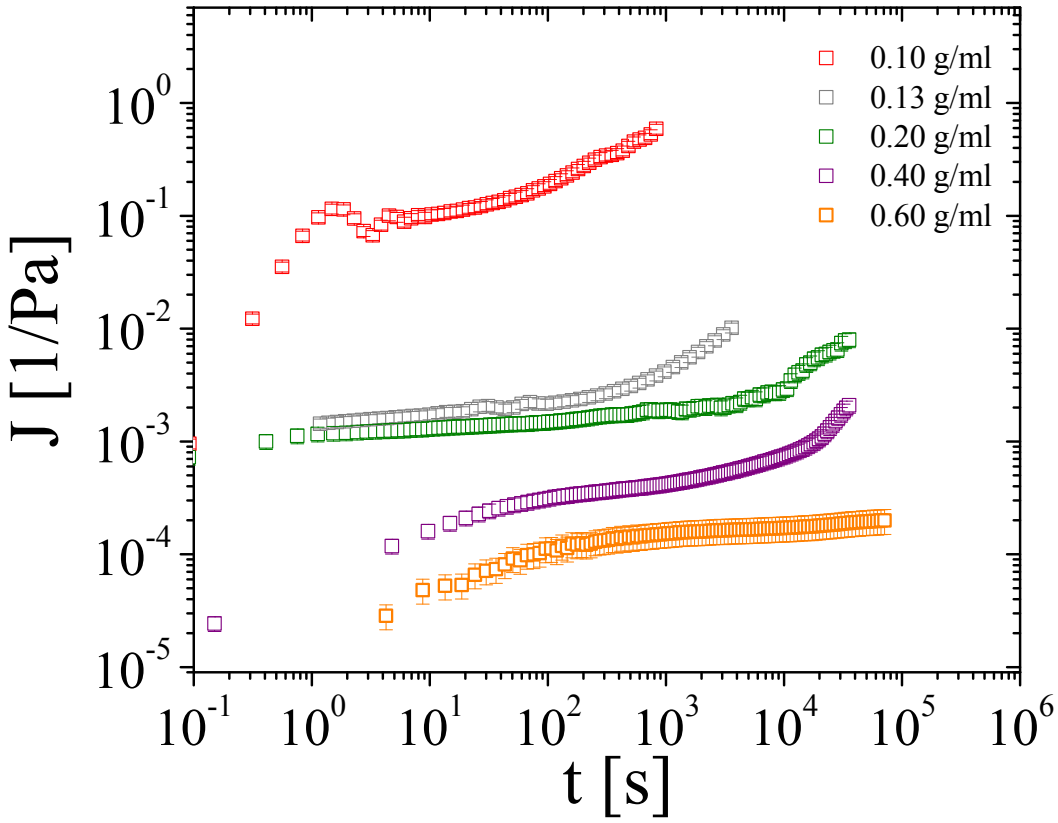

Figure S7. Creep compliance against time at different concentrations: from 0.1 g/ml to 0.6 g/ml. All the experiments were performed at 25 °C.

SI8. High-frequency rheometry

High-frequency rheometry was performed by means of a home-made piezorheometer for the solutions at 0.13, 0.23 and 0.4 g/ml.[13,14] It consists of a set of identical piezo-ceramics PICA™ (PI, Germany), one used as a shear actuator, and the other as a strain sensor. Excitation of the moving plate is exerted by the actuator which provides a sinusoidal voltage waveform with a certain amplitude. The sensing ceramic receives the stress waveform causing charge generation due to the inverse piezoelectric effect. The sensing cell outputs a proportional voltage waveform that can be correlated to the excitation one. The correlation between the two waveforms as input and output allows eventually to extract an amplitude ratio (directly proportional to the complex modulus) and the phase angle.[15]

SI9. Brownian Dynamics Simulations

Nanorods were modeled as a linear, rigid assembly of beads as depicted in Figure S8. The spheres are rigidly connected and the bond length between spheres in each rod was chosen to be the radius of the sphere. In this way, the spheres were overlapping such that the excluded volume was closer to that of a true, smooth spherocylinder compared to, say, a tangent bead model where the beads are

connected at a distance of 2R, which is more common in practice. We consider this to be a coarse-grained representation of a spherocylinder that captures the geometry and anisotropy of interparticle interactions quite well. Note that this model is not a perfect descriptor of the real experimental system as it is missing a number of features including a finite bending modulus of the rods and a uniform scattering cross section along the length of the rod. On the other hand, it is capable of representing some essential features such as particle shape, dispersity, and softness of interactions.

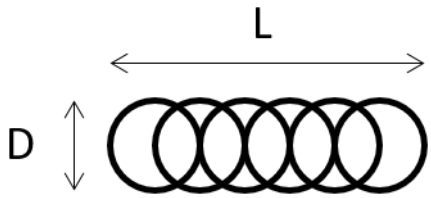

Figure S8. Scheme of modeled nanocylinders.

The polydispersity index (PDI) is defined as

$$PDI = \frac{variance}{mean^2} + 1 \qquad \text{(S2)}$$

This is known from the experimental system and is equal to 1.3. A lognormal distribution of lengths was assumed with parameters given by

$$\mu = \log(\overline{L}) - 0.5\log(PDI) \qquad \text{(S3)}$$

where log(PDI) represents the variance σ^2 and $\overline{L}$ is the mean length, which was set to the experimental value of 6. The distributions are illustrated below in terms of aspect ratio and number of beads in Figure S9.

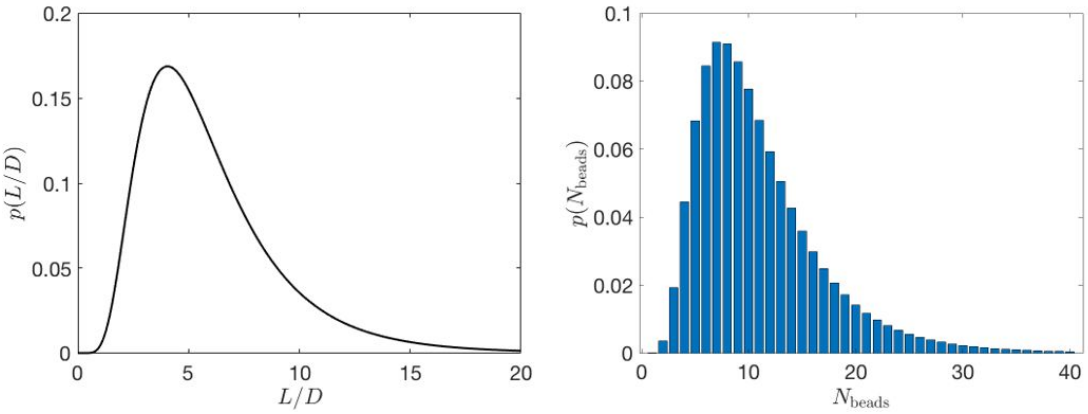

Figure S9. Lognormal distributions of particle aspect ratio and number of beads per nanocylinder.

Particles were integrated according to rigid-body Brownian dynamics with a time step of $\Delta t = 10^{-3}$, and interparticle interactions were given by a custom repulsive interaction potential with tunable softness parameter *k* as:

$$\frac{U}{k_B T} = \frac{(D - 2R_c)^k}{(r - 2R_c)^k} \tag{S4}$$

where U and $k_B T$ are the internal and thermal energies respectively, D is the diameter of the rod, R_c is the radius of the hard core, and r is the interparticle distance. Note that this potential is infinitely stiff when hard cores overlap. Finally, k is the softness parameter: the lower the value, the softer the potential will be. The force can be written as

$$\frac{F}{k_B T} = -\nabla \frac{U}{k_B T} = \frac{k(D - 2R_c)^k}{(r - 2R_c)^{k+1}} \hat{r} \tag{S5}$$

The interaction potential and the effect of the softness parameter k are illustrated in Figure S10.

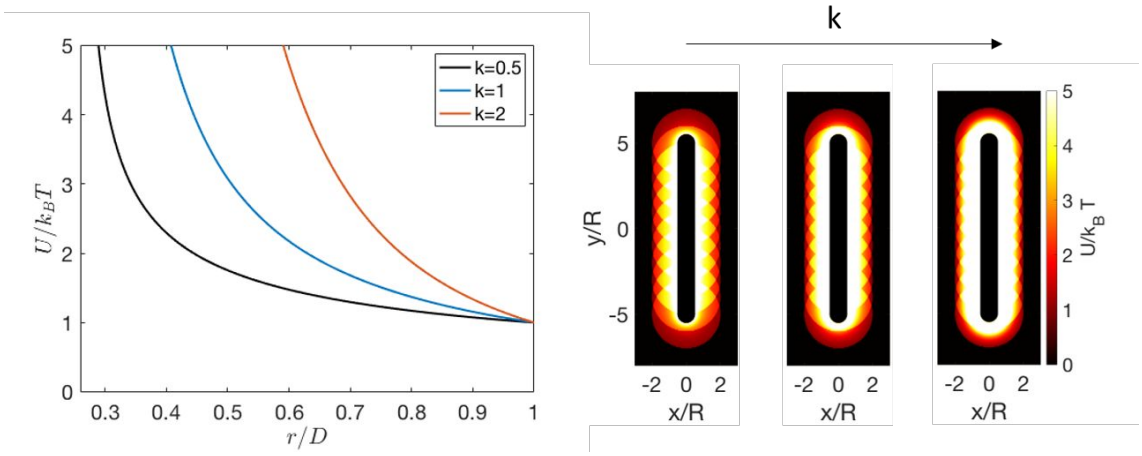

Figure S10. Interaction potential and the effect of softness.

Once the polydispersity and the potential was defined, N=1000 nanocylinders were initially placed in a simulation box (with periodic boundary conditions) on a lattice with random orientations such that no two rods were touching. The system was then equilibrated over a time period of t=500 particle diffusion times, half of which were spent slowly shrinking the simulation box to achieve the desired volume fraction. Figure S11 depicts this equilibration scheme.

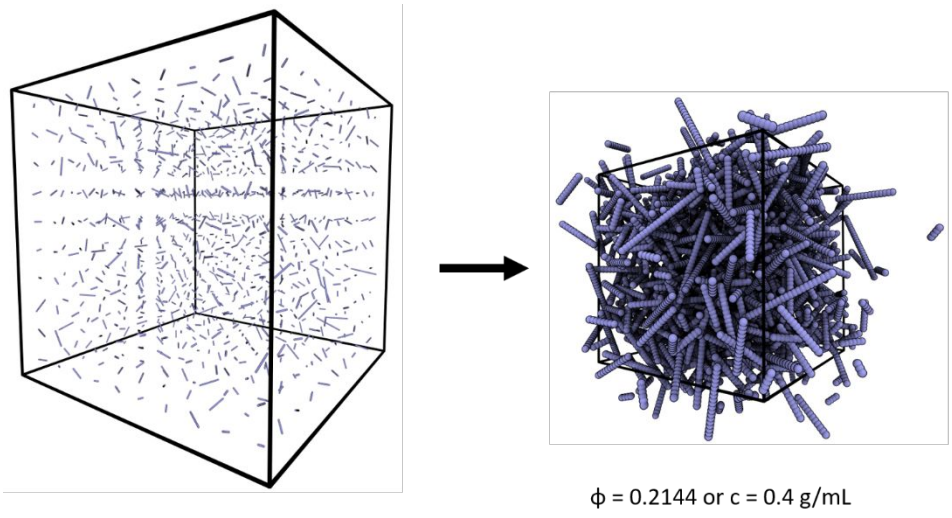

Figure S11. Equilibration scheme of N=1000 cylinders at 0.4 g/ml.

Production runs were then conducted for t=250 diffusion times, over which 100 snapshots were taken in order to calculate the equilibrium static structure factor.

SI10. Shell interpenetration at high concentrations

The presence of a plateau in the storage modulus at high frequencies (Figure 4 of main text) suggests the presence of entanglements between chains. In fact, the high-frequency crossover refers to the relaxation time of an entanglement strand and the plateau corresponds to a network formed by the interpenetrated grafted chains. The procedure we used is reported below for a 40 wt% suspension of nanocylinders in DEP and it is based on the recent work of Wagner et al.[16] It involves the following steps:

1) We determine the concentration of polystyrene, PS (C_{PS}), in the solution (0.79 % of the total mass of the particle is comprised by PS)
2) We estimate the glass transition temperature (T_g) of a PS solution at C_{PS} by using the Flory-Fox equation.
3) By knowing the T_g of PS melts (molar mass M=111 kg/mol) we can compute the difference in T_g as

$$\Delta T_g = T_{g,melt}(M) - T_{g,solution}(M, C_{PS}) \qquad \text{(S6)}$$

(note that the T_g of the solutions, considering only the PS, goes from -12 °C at 0.76 g/ml to -86 °C at 0.1 g/ml. All measurements were performed at 25 °C, well above the T_g of equivalent PS solutions).

4) We build the master curve of PS melt (Figure S12, which also indicates the characteristic relaxation times).

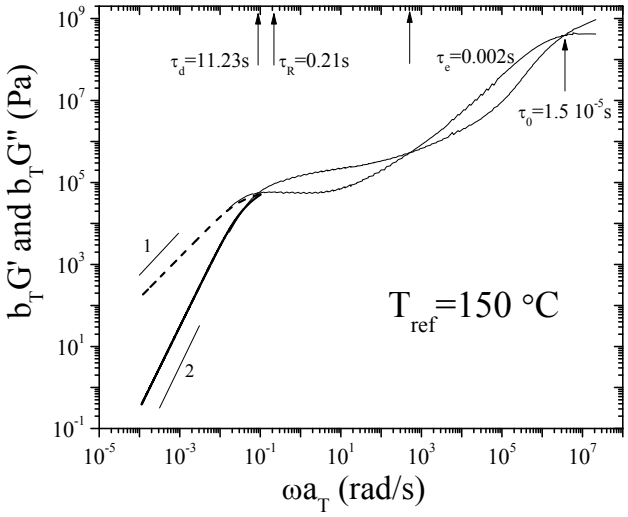

Figure S12: Master curve of PS melt 111 kg/mol at a reference temperature T_{ref}=150^{0}C.

5) We use the William-Landel-Ferry equation below to shift the relaxation time of an entanglement strand (τ_e) to the solution temperature and we obtained a τ_e=3.6 10^{-4} s or a frequency ω_e=2800 rad/s.

$$\log(a_T) = \frac{C_1(T + \Delta T_g - T_{ref})}{C_2 + (T + \Delta T_g - T_{ref})} - \frac{C_1 \Delta T_g}{C_2 + \Delta T_g} \qquad \text{(S7)}$$

The plot below (Figure S13) shows that the τ_e found through this simple calculation is in agreement with the crossover time exhibited by the high-frequency data. This corroborates the fact that indeed, the high-frequency response is dominated by entanglements among grafted chains.

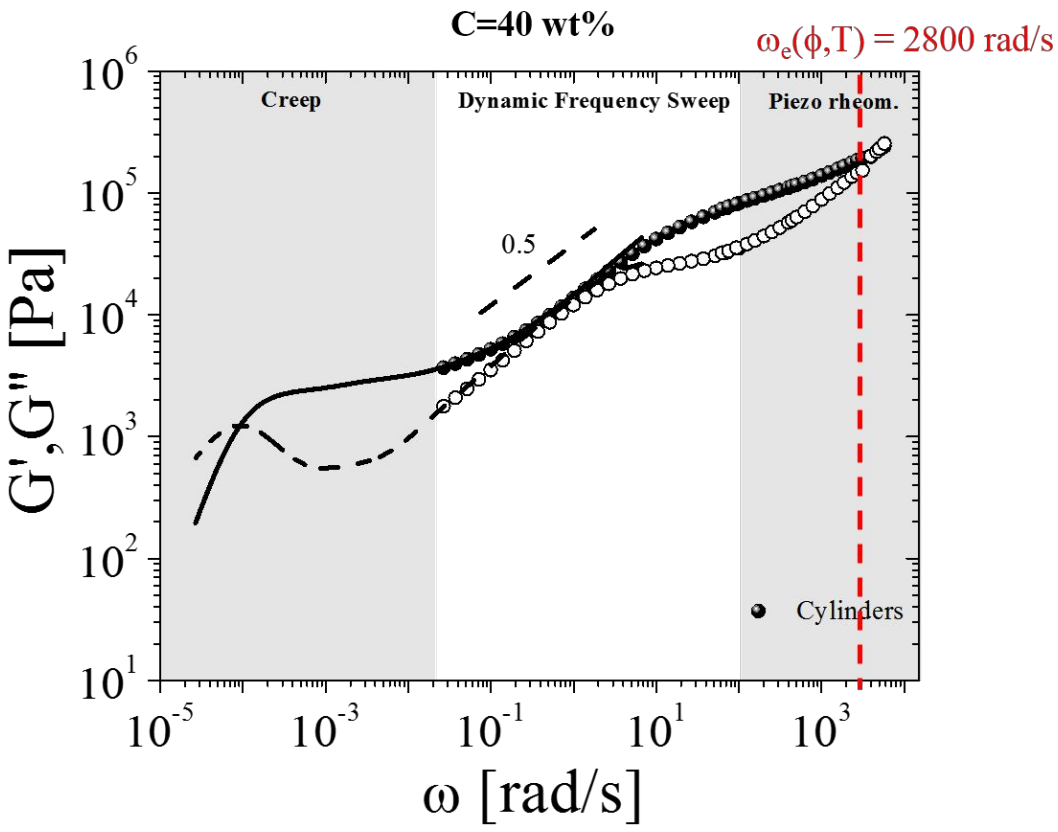

Figure S13: Frequency-dependent linear viscoelastic moduli for nanocylinder solution (40% wt) at 25^{0}C. The conventional dynamic frequency sweep measurements have been complemented by creep (low-frequencies) and piezo-rheomery (hight frequencies) as discussed in the main text.

References

(1) Aragon, S. R.; Pecora, R. Theory of Dynamic Light Scattering from Polydisperse Systems. *The Journal of Chemical Physics* **1976**, *64* (6), 2395–2404.

(2) Bates, M. A.; Frenkel, D. Influence of Polydispersity on the Phase Behavior of Colloidal Liquid Crystals: A Monte Carlo Simulation Study. *The Journal of chemical physics* **1998**, *109* (14), 6193–6199.

(3) Ruan, Y.; Gao, L.; Yao, D.; Zhang, K.; Zhang, B.; Chen, Y.; Liu, C.-Y. Polymer-Grafted Nanoparticles with Precisely Controlled Structures. *Acs Macro Letters* **2015**, *4* (10), 1067–1071.

(4) Berne, B. J.; Pecora, R. Dynamic Light Scattering with Applications to Biology, Chemistry and Physics. *New York: Wiley* **1976**, *1*, 1.

(5) Kang, K.; Dhont, J. K. G. Glass Transition in Suspensions of Charged Rods: Structural Arrest and Texture Dynamics. *Physical review letters* **2013**, *110* (1), 015901.

(6) Binder, K.; Milchev, A. Polymer Brushes on Flat and Curved Surfaces: How Computer Simulations Can Help to Test Theories and to Interpret Experiments. *Journal of Polymer Science Part B: Polymer Physics* **2012**, *50* (22), 1515–1555.

(7) Rubinstein, M.; Colby, R. H. *Polymer Physics*; Oxford University Press New York, 2003; Vol. 23.

(8) Kontopoulou, M. *Applied Polymer Rheology: Polymeric Fluids with Industrial Applications*; John Wiley & Sons, 2011.

(9) Weese, J. A Regularization Method for Nonlinear Ill-Posed Problems. *Computer Physics Communications* **1993**, *77* (3), 429–440.

(10) Friedrich, C.; Honerkamp, J.; Weese, J. New Ill-Posed Problems in Rheology. *Rheologica acta* **1996**, *35* (2), 186–193.

(11) Honerkamp, J.; Weese, J. A Nonlinear Regularization Method for the Calculation of Relaxation Spectra. *Rheologica acta* **1993**, *32* (1), 65–73.

(12) Roths, T.; Marth, M.; Weese, J.; Honerkamp, J. A Generalized Regularization Method for Nonlinear Ill-Posed Problems Enhanced for Nonlinear Regularization Terms. *Computer physics communications* **2001**, *139* (3), 279–296.

(13) Roth, M.; D'Acunzi, M.; Vollmer, D.; Auernhammer, G. K. Viscoelastic Rheology of Colloid-Liquid Crystal Composites. *The Journal of chemical physics* **2010**, *132* (12), 124702.

(14) Yamamoto, J.; Nakamura, H.; Okano, K. Apparatus for Measurement of Complex Shear Modulus of Liquid Crystals at Low Frequencies. *Japanese Journal of Applied Physics* **1987**, *26* (S1), 29.

(15) Athanasiou, T.; Auernhammer, G. K.; Vlassopoulos, D.; Petekidis, G. A High-Frequency Piezoelectric Rheometer with Validation of the Loss Angle Measuring Loop: Application to Polymer Melts and Colloidal Glasses. *Rheologica Acta* **2019**, *58* (9), 619–637.

(16) Wagner, M. H.; Narimissa, E.; Rolón-Garrido, V. H. From Melt to Solution: Scaling Relations for Concentrated Polystyrene Solutions. *Journal of Rheology* **2015**, *59* (4), 1113–1130.